https://doi.org/10.5194/egusphere-2024-2716
Preprint. Discussion started: 2 October 2024


# Atmospheric horizontal gradients measured with eight co-located GNSS stations and a microwave radiometer

Tong Ning[1] and Gunnar Elgered[2]

[1]Lantmäteriet (The Swedish Mapping, Cadastral and Land Registration Authority), SE-80182, Gävle, Sweden
[2]Department of Space, Earth and Environment, Chalmers University of Technology, Onsala Space Observatory, SE-43992 Onsala, Sweden.

**Correspondence:** T. Ning (tong.ning@lm.se)

**Abstract.**

We have used eight co-located GNSS stations, with different antenna mounts, to estimate atmospheric signal propagation delays in the zenith direction and linear horizontal gradients. The gradients are compared with the results from a water vapour radiometer (WVR). Water drops in the atmosphere has a negative influence on the retrieval accuracy of the WVR. Hence we see a better agreement using WVR data with a liquid water content (LWC) less than 0.05 mm compared to when LWC values of up to 0.7 mm are included. We have used two different constraints when estimating the linear gradients from the GNSS data. Using a weak constraint enhances the GNSS estimates to track large gradients of short duration at the cost of increased formal errors. To mitigate random noise in the GNSS data, we adopted a fusion approach averaging estimates from the GNSS stations. This resulted in significant improvements for the agreement with WVR data, a maximum of 17 % increase in the correlation and an 14 % reduction in the root-mean-square (rms) difference for the east gradients. The corresponding values for the north gradients are both 25 %. Overall, no large differences in terms of quality is observed for the eight GNSS stations. However, one station shows slightly poorer agreement for the north gradients compared to the others. This is attributed to the station's proximity to a radio telescope, which causes data loss of observations at low elevation angles in the south-south-west direction.

## 1 Introduction

After decades of development, the data acquired from continuously operating Global Navigation Satellite System (GNSS) stations are widely used in various applications. For example, the BIFROST (Baseline Inferences for Fennoscandian Rebound Observations Sea Level and Tectonics) project combines networks of continuously operating GPS receivers in the Nordic countries to establish a useful three-dimensional measurement of the movements in the earth crust which is used to constrain models of the GIA (glacial isostatic adjustment) process in Fennoscandia (Kierulf et al., 2019). For such geodetic applications, it is recommended to estimate the Zenith Total Delays (ZTD) together with the horizontal gradients in a GNSS data processing.

ZTDs obtained from GNSS observations by ground-based receiver stations in the Nordic countries are used within a state-of-the-art km-scale numerical weather prediction system (Lindskog et al., 2017). The investigation demonstrates that the assimilation of the GNSS ZTD can benefit from more general data assimilation enhancements. Thundathil et al. (2024) also found that

https://doi.org/10.5194/egusphere-2024-2716
Preprint. Discussion started: 2 October 2024


the combined assimilation of horizontal gradients together with the ZTD into the Weather Research and Forecasting (WRF) model results in a clear improvement in the humidity field at altitudes above 2.5 km and therefore they recommended further GNSS gradient assimilation studies. With a relatively high temporal resolution, continuously improving spatial density, and less expensive receivers, ground-based GNSS networks are also used to monitor the long-term changes in the atmospheric water vapour (e.g., *Chen and Liu* 2016 and *Parracho et al.* 2018). In addition, the satellite geometries of the GNSS measurements have been continuously improved through multi-GNSS constellations and it is benefit for the estimation of the gradients. Ning and Elgered (2021) found that relative to the GPS-only solution, the solution using GPS, Glonass, and Galileo data resulted in an increase in the correlation coefficient of 11 % for the east gradient and 20 % for the north gradient.

The Swedish GNSS network of permanent reference stations, SWEPOS$^{TM}$, was declared operational for post-processing applications and support for real-time positioning with metre accuracy in 1998. It is operated by Lantmäteriet (Swedish Mapping, Cadastral and Land Registration Authority). Currently (August, 2024) the SWEPOS network consists of 483 GNSS permanent reference stations where 21 concrete pillar stations that serve as the backbone for SWEREF 99 (the national reference frame). To keep the time series of the 21 fundamental stations consistent, the antennas of these pillar stations will not be changed as long as they work properly. To be able to track all new signals, such as Galileo and GPS L5 properly, starting from 2012 a second monument, a steel grid mast, was installed closely to each pillar station with a newer antenna (LEIAR25.R3) and a radome (LEIT). In addition, there are other types of antennas, radomes, and monuments used in the SWEPOS network. It is therefore of interest to investigate the performance of different station designs.

We used eight GNSS stations of different designs, co-located at the Onsala Space Observatory, to estimate linear horizontal gradients. The specifications of the GNSS stations and their data processing are described in Section 2.1 and the WVR data acquisition and processing are presented in Section 2.2. In Section 3.1 we first present the agreement of the horizontal gradients between the eight GNSS stations. Thereafter, in Section 3.2 the GNSS data are compared to the WVR data acquired during 5 min periods. This included an assessment of the impact of the retrieval accuracy of the equivalent gradients from WVR data due to the dependence on the estimated liquid water content (LWC) from the WVR. In Section 3.3 we study the impact of using a weaker constraint for the random walk process of the GNSS gradient time series. In order to reduce the random noise in the GNSS data we averaged GNSS data obtained from the different stations and compared with the WVR data. This is similar to what was done by Wang et al. (2024) where they averaged observations in order to reduce the noise from inexpensive co-located GNSS receivers. The conclusions are given in Section 4.

## 2 Datasets

### 2.1 GNSS

The eight GNSS stations and their locations are shown in Figures 1 and 2. Table 1 summarizes the specifications of the stations. ONSA is one of the 21 SWEPOS fundamental stations, but with a 1 m concrete pillar, instead of 3 m, and a microwave absorbing plate below the antenna. ONS1 is one of the 21 secondary stations which are installed close to each pillar station and has a 3 m steel mast. Surrounding to the Onsala Twin Telescopes (OTT) for geodetic very long baseline interferometry

https://doi.org/10.5194/egusphere-2024-2716
Preprint. Discussion started: 2 October 2024


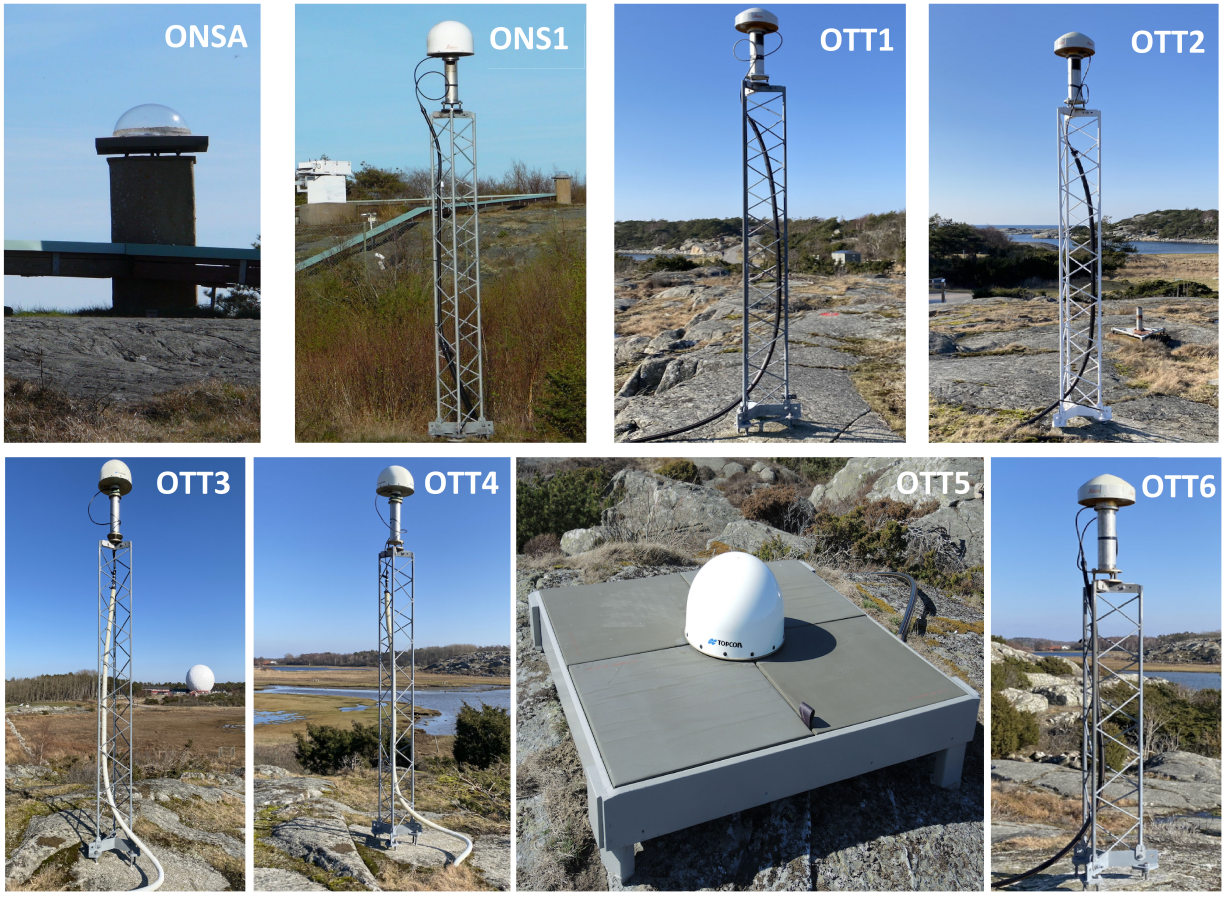


**Figure 1.** The eight GNSS stations (from left to right) are ONSA, ONS1, OTT1 to OTT6.

(VLBI), an additional 6 GNSS stations have been deployed. OTT1, OTT2, OTT3, OTT4, and OTT6 has an installation similar to ONS1. The design of the OTT5 station is made significantly different from the others. The antenna is mounted directly above the bedrock with a plate of microwave absorbing material below. All eight GNSS stations have hemispheric radomes. Many studies have shown that a hemispheric radome design is preferred in order to minimize errors in the estimated zenith wet delay (ZWD) and coordinates (e.g., *Emardson et al.* 2000 and *Ning et al.* 2011). All six OTT stations underwent a receiver change in February 2022 to enable tracking of all Beidou satellites. To ensure consistent data and satellite geometry across all the eight stations, we decided to include data acquired from March 2022 to December 2023.

The GNSS data processing was carried out using GipsyX v.2.0 (Bertiger et al., 2020) with the Precise Point Positioning (PPP) strategy (Zumberge et al., 1997). The input to the data processing was ionospheric free linear combinations formed by acquired GNSS phase-delay observations while the output included station coordinates, clock biases, and atmospheric parameters. The final multi-GNSS orbit and clock products were provided by the Center for Orbit Determination in Europe (CODE) (Prange et al., 2020). The slant delays were mapped to the zenith using the Vienna Mapping Function 1 (VMF1) (Boehm et al., 2006).

https://doi.org/10.5194/egusphere-2024-2716
Preprint. Discussion started: 2 October 2024


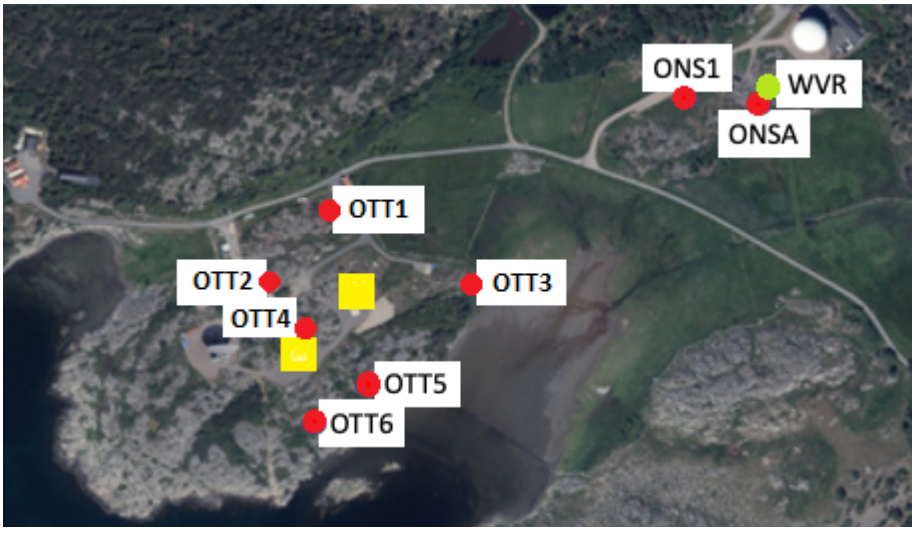


**Figure 2.** The locations of the eight GNSS stations (red circles), the WVR (green circle), and the twin telescopes used for geodetic VLBI (yellow squares). Distances to the WVR are given in Table 1.

**Table 1.** The specifications of the GNSS stations.

| Station | Antenna | Radome | Receiver | Pillar | Height [m][a] | Distance [m][b] |
|---|---|---|---|---|---|---|
| ONSA | AOADM/M_B | OSOD | Sept Polarx5tr | 1 m concrete | 10.2 | 11 |
| ONS1 | LEIAR25.R3 | LEIT | Trimble alloy | 3 m steel | 8.1 | 54 |
| OTT1 | LEIAR20 | LEIM | Trimble NetR9 | 3 m steel | 9.3 | 404 |
| OTT2 | LEIAR20 | LEIM | Trimble NetR9 | 3 m steel | 10.5 | 441 |
| OTT3 | TPSCR.G5 | TPSH | Trimble NetR9 | 3 m steel | 8.8 | 315 |
| OTT4 | LEIAR20 | LEIM | Trimble NetR9 | 3 m steel | 10.9 | 438 |
| OTT5 | TPSCR.G5 | TPSH | Trimble NetR9 | None | 12.4 | 420 |
| OTT6 | LEIAR20 | LEIM | Trimble NetR9 | 2 m steel | 11.0 | 474 |

[a] The heights are referenced to the geoid.

[b] The distance from the location of the WVR.

The ZTD and the horizontal delay gradients were estimated every 5 min using a random walk model with constraints of 10 mm$\sqrt{\text{h}}^{-1}$ and 0.3 mm$\sqrt{\text{h}}^{-1}$, for standard deviations (SD), respectively. Equal weighting of the observations was applied. The constraint value used for the ZTD was given by Jarlemark et al. (1998) where they found a temporal variability in the wet delay, derived from 71 days of WVR measurements, varying in the interval 3–22 mm$\sqrt{\text{h}}^{-1}$ at the Onsala site. In GipsyX, the default SD for gradients is 0.3 mm$\sqrt{\text{h}}^{-1}$. In order to assess the impact on the gradient estimation, we have also applied a weaker constraint of 2.0 mm$\sqrt{\text{h}}^{-1}$.

https://doi.org/10.5194/egusphere-2024-2716
Preprint. Discussion started: 2 October 2024


We used the model presented by Bar-Sever et al. (1998) for the gradient estimation:

$$S(\epsilon,\phi) = m(\epsilon)\,[Z + cot(\epsilon)(G_n\,cos(\phi) + G_e\,sin(\phi))] \quad (1)$$

where $S(\epsilon,\phi)$ is a slant delay for a certain elevation and azimuth angle; $Z$ and $m(\epsilon)$ are the zenith delay and the elevation mapping function; $G_n$ and $G_e$ are the north and east horizontal gradient, respectively. Given that the WVR only provide the wet gradient while the GNSS gradient is the sum of the wet and the hydrostatic components, we need to subtract the hydrostatic component from the GNSS estimates to be able to compare with the WVR gradients. The horizontal hydrostatic gradients used were calculated by VMF Data Server (2024) which is based on the ERA-Interim numerical weather model.

### 2.2 Water Vapour Radiometer (WVR)

The WVR was designed in order to provide independent estimates of the wet propagation delays for space geodetic applications. It is fully steerable and measures the emission from the sky at 20.65 GHz and 31.63 GHz. These observations are used to derive the equivalent ZWD and the liquid water content (LWC). More detailed specifications are given by Elgered et al. (2019).

The microwave radiometer has a maximum distance of 474 m to the GNSS stations (see Table 1). The height difference to ONSA is less than 0.5 m. Because the maximum height difference between the WVR and all the other GNSS stations is 2.2 m, no attempt was made to make any model based correction as a function of the antenna height of the stations.

From 2022 the observations were scheduled in a 2 min long cycle with the ambition to sample the whole atmosphere at elevation angles above 25°. For this work, however, the highest temporal resolution is 5 min. Furthermore, from 22 August 2023 the observational cycle was changed to a much more dense sampling of the sky during a cycle of 5 min. The WVR observations on the sky are illustrated in Fig. 3.

A four-parameter model was used to estimate a mean ZWD, a linear trend in the ZWD, and east and north linear horizontal gradients over a 5 min period (Davis et al., 1993). No constraint between estimates in adjacent periods was applied. Before the final processing of the WVR raw data, periods of rain, indicated by a rain sensor at the site, were identified. Data were removed from 5 min before the rain started until at least 15 min after it stopped. The amount of data removed after each rain event was based on a subjective inspection of the ZWD time series. Depending on the weather conditions the time needed for water drops to disappear on the WVR feeds varies.

In order to apply the four-parameter model, we required that each observation used had an estimated equivalent zenith LWC $<$0.7 mm. We also required that at least 30 observations were available in each 5 min interval during the period from March 2022 to August 2023. From September 2023, when the sample rate had been increased, this requirement was increased to at least 75 observations. The two different sampling rates did not show any significant impact on biases in the gradient time series because they cover similar elevation ranges. Gradient biases are further discussed in Section 3.2.

A second WVR dataset was also produced where all individual WVR observations resulting in a LWC $>$ 0.05 mm were ignored. The reason for applying this strict editing is to have as accurate estimates as possible in the comparisons to the results from the eight GNSS stations. Since the WVR estimates are fully independent of the corresponding estimates from the GNSS data they form a suitable reference dataset.

https://doi.org/10.5194/egusphere-2024-2716
Preprint. Discussion started: 2 October 2024


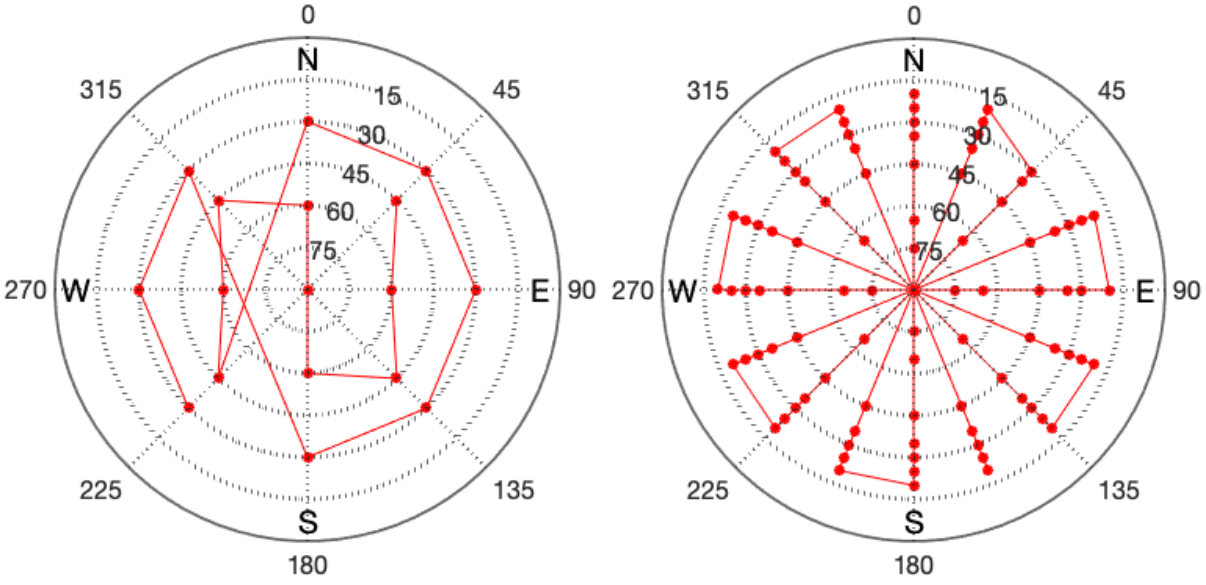


**Figure 3.** From 1 March 2022 to 22 August 2023 the WVR made 17 observations in a 2 min cycle (left). Thereafter, a 5 min cycle was used with 90 observations (right), and from 15 November an additional 7 observations were added, to tune the cycle to 5 min, within a couple of seconds. The zenith point is only measured once in each cycle.

### 2.3 The different datasets used

Due to the sometimes rapid variations in the horizontal gradients, as well as due to data gaps, synchronization of the datasets from the stations being compared is necessary. In addition the pure GNSS dataset we use four different datasets from the WVR. Figure 4 shows the number of available data points from GNSS and WVR when synchronised.

Table 2 summarizes the statistics of the formal error for the estimated gradients. As expected, applying a weak constraint in the GNSS data processing increases the formal error of the gradient. ONSA has the smallest formal errors. It is equipped with microwave-absorbing material, below the antenna above the metal plate used for the antenna mounting, which likely reduces unwanted multipath effects. It is also interesting to note that OTT5 has comparable formal errors to the other stations, although the antenna is mounted directly above the bedrock. The WVR data exhibit slightly larger formal errors for both the east and the north gradients when the larger threshold (0.7 mm) for the LWC is used. The formal errors of the WVR gradients are slightly reduced when the amplitude of the total gradient is less than 0.5 mm but this is not the case for the relative formal errors.

An overview of the data in terms of monthly means of the wet gradient amplitude is shown in Figure 5 for the ONSA station. It is noted that the WVR data result in much larger gradients. Additionally, the amplitudes from two GNSS solutions with different constraints are different but show a strong correlation with each other. This result is consistent with findings from Elgered et al. (2019), which concluded that the constraints and the sampling of different air masses are likely explanations for the differences in gradient amplitudes estimated from the GNSS and the WVR data.

https://doi.org/10.5194/egusphere-2024-2716
Preprint. Discussion started: 2 October 2024


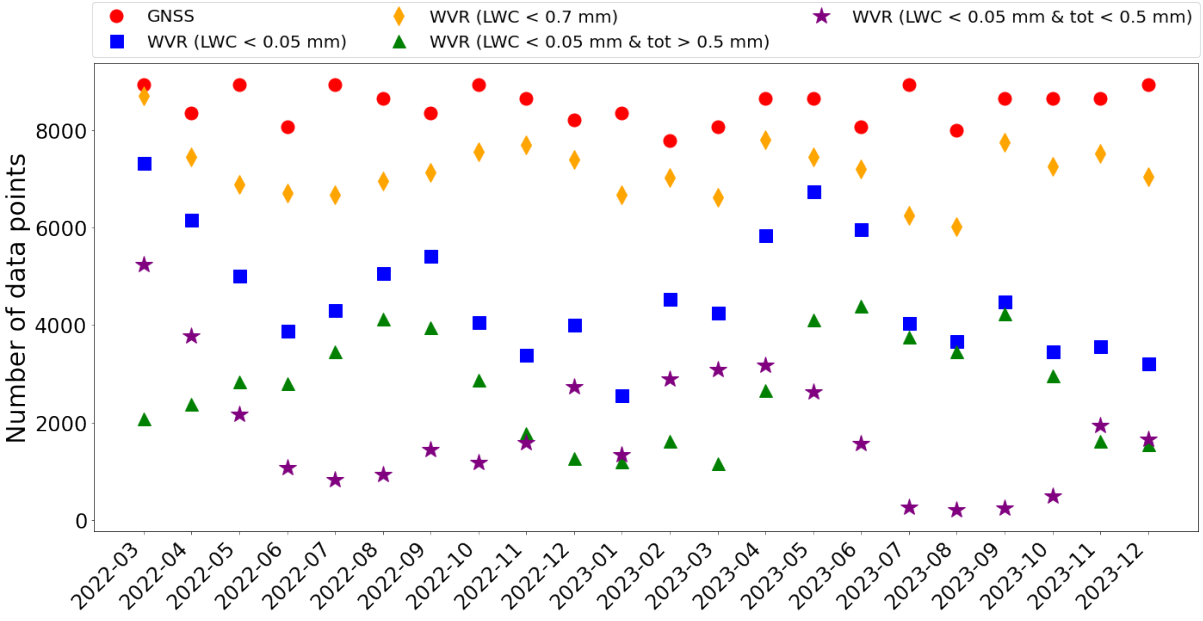


**Figure 4.** Number of simultaneous data points for all 8 GNSS stations is 187,269; available data points while LWC $< 0.05$ mm or $< 0.7$ mm is 100,938 and 157,670, respectively. The smaller dataset, when LWC $< 0.05$ mm, is divided into two datasets when the total gradient amplitude ($\sqrt{G_e^2 + G_n^2}$) $> 0.5$ mm or $< 0.5$ mm results in 60,416 and 40,522 data points, respectively.

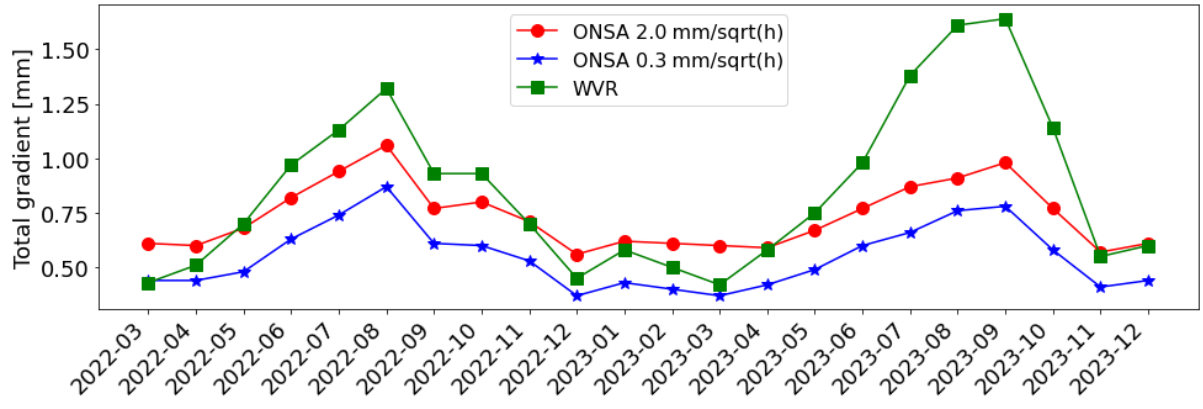


**Figure 5.** The monthly means of wet gradient amplitudes ($\sqrt{G_e^2 + G_n^2}$) from the WVR and the two GNSS solutions using the two different constraints, 0.3 and 2.0 mm$\sqrt{\text{h}}^{-1}$ respectively.

125 To provide some details about the estimated gradients, Figure 6 shows the time series of the gradients from 00 UT on 1 August to 24 UT on 4 August, 2022, from the WVR and from the GNSS data applying the two different constraints. When a weak constraint is applied, there is an improvement in tracking larger gradients. However, the overall gradients given by a

https://doi.org/10.5194/egusphere-2024-2716
Preprint. Discussion started: 2 October 2024


**Table 2.** The formal error, mean and SD (in parentheses), for GNSS and WVR gradients.

| Station | Constraint of 0.3 mm$\sqrt{\text{h}}^{-1}$ | | Constraint of 2.0 mm$\sqrt{\text{h}}^{-1}$ | |
|---|---|---|---|---|
| | EG [mm] | NG [mm] | EG [mm] | NG [mm] |
| ONSA | 0.14 (0.03) | 0.15 (0.03) | 0.30 (0.08) | 0.32 (0.08) |
| ONS1 | 0.16 (0.03) | 0.18 (0.03) | 0.33 (0.12) | 0.35 (0.13) |
| OTT1 | 0.16 (0.03) | 0.18 (0.03) | 0.36 (0.12) | 0.39 (0.12) |
| OTT2 | 0.17 (0.03) | 0.17 (0.03) | 0.36 (0.09) | 0.38 (0.10) |
| OTT3 | 0.16 (0.03) | 0.16 (0.03) | 0.35 (0.13) | 0.36 (0.13) |
| OTT4 | 0.17 (0.03) | 0.19 (0.03) | 0.37 (0.10) | 0.41 (0.12) |
| OTT5 | 0.16 (0.03) | 0.17 (0.03) | 0.37 (0.13) | 0.38 (0.14) |
| OTT6 | 0.18 (0.03) | 0.19 (0.03) | 0.40 (0.13) | 0.43 (0.13) |
| *Each WVR gradient is independent on adjacent values in the estimation process* | | | | |
| WVR, LWC $<$ 0.7 mm | | | 0.10 (0.12) | 0.09 (0.11) |
| WVR, LWC $<$ 0.05 mm | | | 0.07 (0.04) | 0.06 (0.04) |
| WVR, LWC $<$ 0.05 mm + tot. grad. ampl.$>$0.5 mm | | | 0.07 (0.04) | 0.07 (0.04) |
| WVR, LWC $<$ 0.05 mm + tot. grad. ampl.$<$0.5 mm | | | 0.06 (0.02) | 0.05 (0.02) |

weak constraint also show greater scatter compared to those given by a strong constraint. This issue is discussed in detail in Section 3.3.

https://doi.org/10.5194/egusphere-2024-2716
Preprint. Discussion started: 2 October 2024


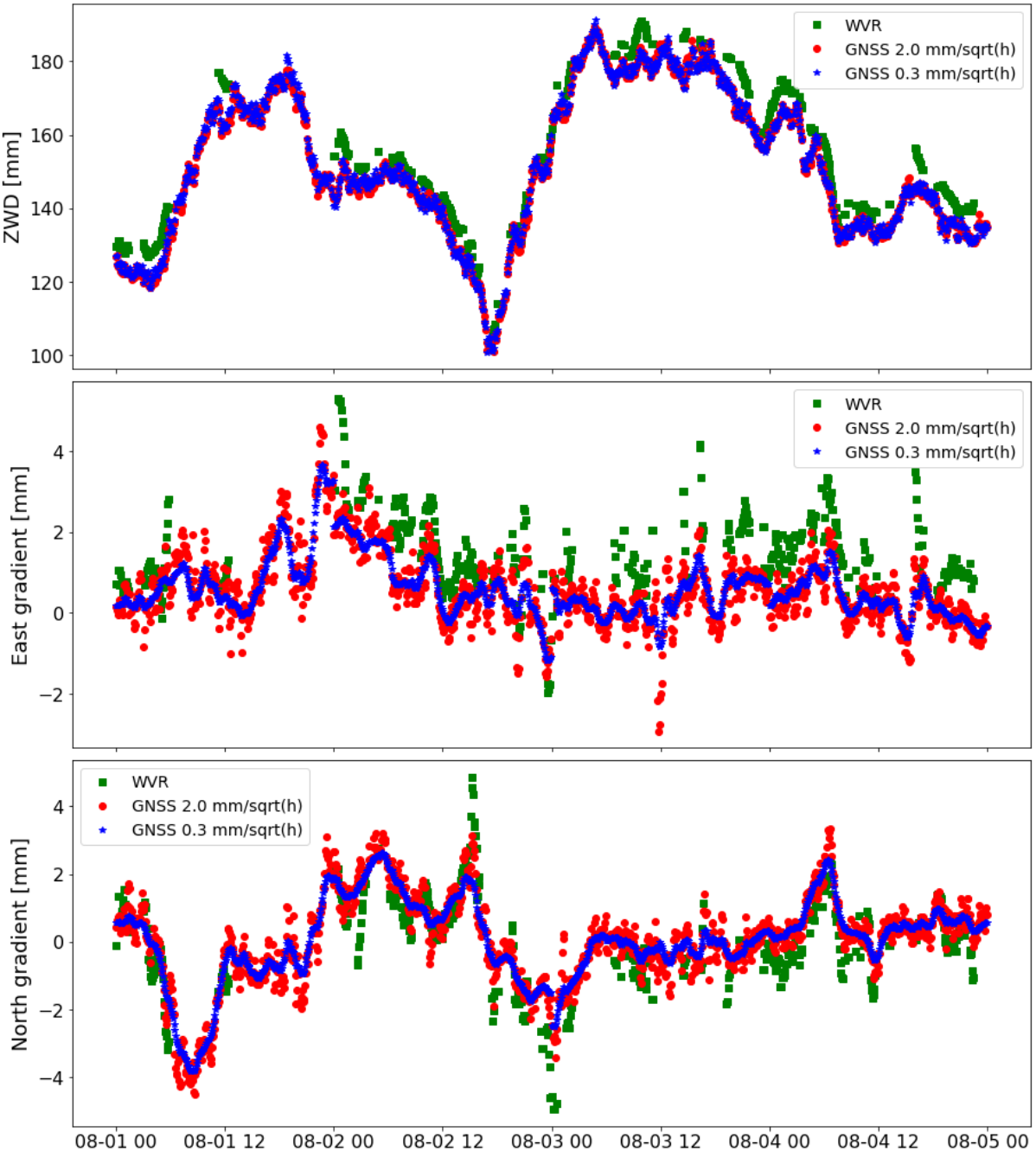


**Figure 6.** Gradient time series for 4 days from WVR and the GNSS solution for ONSA station using two different constraints, 0.3 and 2.0 mm$\sqrt{\text{h}}^{-1}$ respectively.

https://doi.org/10.5194/egusphere-2024-2716
Preprint. Discussion started: 2 October 2024


## 3 Comparison results

### 3.1 GNSS gradients vs GNSS gradients

Initially, we assess the gradients derived from the eight GNSS stations in comparison with one another. We expect a strong agreement, given the similarity in the atmospheric sampling across the all stations and the shared presence of various error sources among them. On the other hand, such pairwise comparison from several co-located stations can also reveal errors from a specific station. The results in terms of root-mean-square (rms) differences and correlations are shown in Table 3. The rms differences are dominated by the standard deviations. The observed biases are of the order of 0.1 mm or less. We observe rather consistent agreements across all stations. The OTT4 station does, however, show slightly larger rms differences and lower correlations in the north gradient as a consequence from less observations in the south-south-west direction caused by the blockage of the VLBI telescope (see Fig. 2).

The OTT5 antenna, mounted directly above the bedrock, gives consistent agreement with other stations showing no clear impact from the environment, such as multipath. This is probably due to the plate of microwave absorbing material placed right below the antenna.

We note that the agreements between ONSA-ONS1 and between the six OTT stations are not significantly better indicating that the longer distances of a few hundred metres are not important when observations are averaged over 5 min intervals.

### 3.2 GNSS gradients vs WVR gradients for LWC $<$ 0.05 or $<$ 0.7 mm

In order to investigate the influence of the amount of liquid water in the atmosphere on the retrieval accuracy of the gradients using the WVR, we have applied two LWC threshold values (0.05 and 0.7 mm) for which individual WVR observations to include in each 5 min estimate of the four-model parameters. Table 4 shows the results from the comparison between the GNSS and the WVR gradients. We chose to present biases, standard deviations, and rms differences because in this case the biases in the east direction cannot be ignored. The biases between the WVR and GNSS are approximately equal to the mean values of the WVR gradients. We expect the true values of the mean gradients to be close to zero over a time period of almost two years. This is also what we see from the GNSS and ERA-Interim results. The explanation for the WVR bias is likely from the uncertainties in the elevation angle, which is of the order of 0.1°. The observations are carried out for azimuth angles between 0° and 180° and observations towards the west are obtained using elevation angles larger than 90° (see Fig. 3). Introducing an offset in the pointing of $-0.1°$ for the lower frequency channel and $+0.1°$ in the other channel, changes the estimated gradient by approximately 0.4 mm. This bias uncertainty in the WVR gradients are however not important when we compare the different GNSS stations and different GNSS solutions to each other relative the WVR gradients.

Although the differences are small, we see that the ONSA station has the best while the OTT4 station exhibits the worst agreement with the WVR estimates for both datasets and for both the east and the north gradients. In the following comparisons are done using WVR gradients obtained from observations with an LWC $<$ 0.05 mm in order to have as high quality as possible.

https://doi.org/10.5194/egusphere-2024-2716
Preprint. Discussion started: 2 October 2024


**Table 3.** Correlation coefficients (upper right triangle) and rms differences in mm (lower left triangle) for horizontal gradients over the whole time period. The best and the worst agreements are highlighted by cyan and red colour, respectively.

| Station | ONSA | ONS1 | OTT1 | OTT2 | OTT3 | OTT4 | OTT5 | OTT6 |
|---|---|---|---|---|---|---|---|---|
| | | | | *East gradient* | | | | |
| ONSA | – | 0.92 | 0.93 | 0.92 | 0.94 | 0.92 | 0.93 | 0.91 |
| ONS1 | 0.24 | – | 0.91 | 0.90 | 0.92 | 0.91 | 0.93 | 0.91 |
| OTT1 | 0.23 | 0.25 | – | 0.93 | 0.93 | 0.93 | 0.92 | 0.91 |
| OTT2 | 0.25 | 0.27 | 0.23 | – | 0.93 | 0.93 | 0.92 | 0.90 |
| OTT3 | 0.23 | 0.27 | 0.23 | 0.26 | – | 0.92 | 0.94 | 0.91 |
| OTT4 | 0.25 | 0.27 | 0.23 | 0.24 | 0.25 | – | 0.92 | 0.91 |
| OTT5 | 0.23 | 0.24 | 0.23 | 0.26 | 0.22 | 0.25 | – | 0.94 |
| OTT6 | 0.25 | 0.25 | 0.25 | 0.27 | 0.26 | 0.26 | 0.21 | – |
| | | | | *North gradient* | | | | |
| ONSA | – | 0.89 | 0.89 | 0.90 | 0.92 | 0.86 | 0.91 | 0.89 |
| ONS1 | 0.26 | – | 0.87 | 0.88 | 0.90 | 0.85 | 0.90 | 0.88 |
| OTT1 | 0.26 | 0.29 | – | 0.91 | 0.91 | 0.88 | 0.89 | 0.88 |
| OTT2 | 0.25 | 0.28 | 0.25 | – | 0.92 | 0.89 | 0.90 | 0.88 |
| OTT3 | 0.22 | 0.25 | 0.23 | 0.23 | – | 0.89 | 0.92 | 0.90 |
| OTT4 | 0.29 | 0.31 | 0.28 | 0.26 | 0.27 | – | 0.86 | 0.85 |
| OTT5 | 0.23 | 0.24 | 0.26 | 0.25 | 0.21 | 0.29 | – | 0.91 |
| OTT6 | 0.27 | 0.27 | 0.29 | 0.27 | 0.26 | 0.31 | 0.24 | – |

### 3.3 GNSS gradients estimated with different constraints

We have applied two different constraints of 0.3 or 2.0 mm$\sqrt{\text{h}}^{-1}$ for the SD in the random walk model for the GNSS gradients. The comparison results to the WVR are presented in Table 5. As already noted in Section 2.3, using a weak constraint enhances the GNSS data tracking large gradients at the cost of larger formal errors. This also affects the agreement between GNSS and WVR gradients, which is confirmed in the table.

Table 5 also includes the agreement results for the two datasets when the total gradient from the WVR is $< 0.5$ mm or $> 0.5$ mm. As expected, these results show that both the correlation and the SD increase when gradients are large. When gradients are very small, there is almost no correlation to be found and the SD shall be just the random errors. When gradients are larger there is also a contribution to the differences from the different sampling of the sky.

To compare the two solutions using different constraints we carried out averaging of the gradients from the individual GNSS stations. As pointed out by Ning et al. (2016) errors in GNSS measurements are random or systematic and random errors are uncorrelated across different stations, and can be reduced through averaging. We started with the gradients from ONSA and averaged them with the ones from ONS1. Thereafter, we added also the gradients from OTT1 to ONSA and ONS1 to form

https://doi.org/10.5194/egusphere-2024-2716
Preprint. Discussion started: 2 October 2024


**Table 4.** Agreement between the horizontal gradients from mutli-GNSS and the WVR, estimated using two different maximum values for the LWC from the WVR. The best and the worst agreements are highlighted by cyan and red colour, respectively.

| Station | Bias | | Standard Deviation | | RMS | | Correlation | |
|---|---|---|---|---|---|---|---|---|
| | EG [mm] | NG [mm] | EG [mm] | NG [mm] | EG [mm] | NG [mm] | EG | NG |
| | | | | *LWC < 0.05 mm* | | | | |
| ONSA | −0.41 | 0.14 | 0.55 | 0.48 | 0.69 | 0.50 | 0.71 | 0.69 |
| ONS1 | −0.44 | 0.15 | 0.57 | 0.51 | 0.72 | 0.53 | 0.67 | 0.64 |
| OTT1 | −0.41 | 0.09 | 0.57 | 0.52 | 0.70 | 0.53 | 0.69 | 0.63 |
| OTT2 | −0.46 | 0.15 | 0.58 | 0.50 | 0.74 | 0.52 | 0.67 | 0.65 |
| OTT3 | −0.33 | 0.12 | 0.57 | 0.49 | 0.66 | 0.50 | 0.69 | 0.67 |
| OTT4 | −0.40 | 0.12 | 0.58 | 0.53 | 0.70 | 0.54 | 0.66 | 0.62 |
| OTT5 | −0.36 | 0.12 | 0.57 | 0.49 | 0.67 | 0.50 | 0.68 | 0.67 |
| OTT6 | −0.42 | 0.19 | 0.58 | 0.51 | 0.72 | 0.54 | 0.66 | 0.65 |
| | | | | *LWC < 0.7 mm* | | | | |
| ONSA | −0.50 | 0.15 | 0.70 | 0.61 | 0.86 | 0.63 | 0.67 | 0.65 |
| ONS1 | −0.53 | 0.17 | 0.72 | 0.64 | 0.89 | 0.66 | 0.64 | 0.61 |
| OTT1 | −0.49 | 0.12 | 0.71 | 0.64 | 0.86 | 0.65 | 0.64 | 0.60 |
| OTT2 | −0.54 | 0.17 | 0.72 | 0.63 | 0.90 | 0.65 | 0.63 | 0.62 |
| OTT3 | −0.42 | 0.14 | 0.71 | 0.62 | 0.82 | 0.64 | 0.65 | 0.64 |
| OTT4 | −0.49 | 0.14 | 0.73 | 0.65 | 0.88 | 0.66 | 0.63 | 0.58 |
| OTT5 | −0.46 | 0.14 | 0.72 | 0.62 | 0.85 | 0.64 | 0.64 | 0.64 |
| OTT6 | −0.50 | 0.21 | 0.73 | 0.63 | 0.88 | 0.66 | 0.63 | 0.61 |

new averages and again assessed the agreement with the WVR. This iterative fusion process progressed further until all eight stations were averaged for comparison with the WVR data. The result obtained when averaging all eight stations is the entry called "fusion" in Table 5. Figure 7 illustrates the agreement obtained when another GNSS station is added to the calculation of the mean value. We notice that while the averaging improve the agreement with the WVR gradients when applying the weak constraint, the effect for the strong constraint is hardly significant. Our interpretation is that the use of the week constraint results in more random errors whereas the errors present in the solution using a strong gradient is dominated by systematic effects.

Finally, since the presence of gradients varies a lot with the weather, and therefore also the seasons, the result for each month is of interest. These correlations and the standard deviations are presented in Figure 8. The monthly results are consistent with the overall result for the whole dataset, although the level of agreement varies with the seasons. The results indicate that for months with large gradients, such as July and August 2022 and September 2023, the weak constraints yield a better correlation

https://doi.org/10.5194/egusphere-2024-2716
Preprint. Discussion started: 2 October 2024


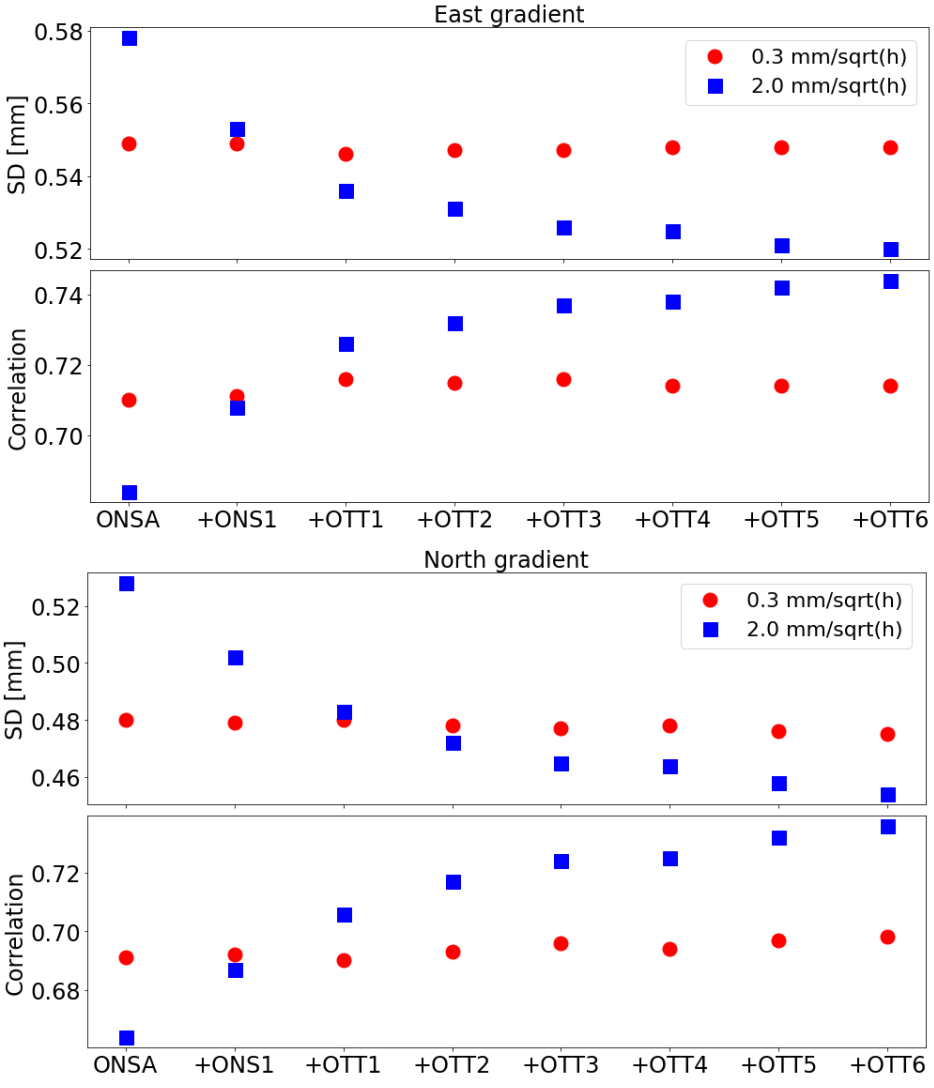


**Figure 7.** Averaged GNSS gradients vs WVR gradients.

185 with the WVR data. However, for months with small gradients, worse correlations are seen due to the dominance of the noise introduced by weak constraints and the smaller dynamic range. This pattern is also observed for the SD results, where weak constraints produce smaller or similar values compared to strong constraints in months with large gradients. Conversely, in months with small gradients, weak constraints result in larger SD as they introduced more noise in the GNSS gradients.

https://doi.org/10.5194/egusphere-2024-2716
Preprint. Discussion started: 2 October 2024


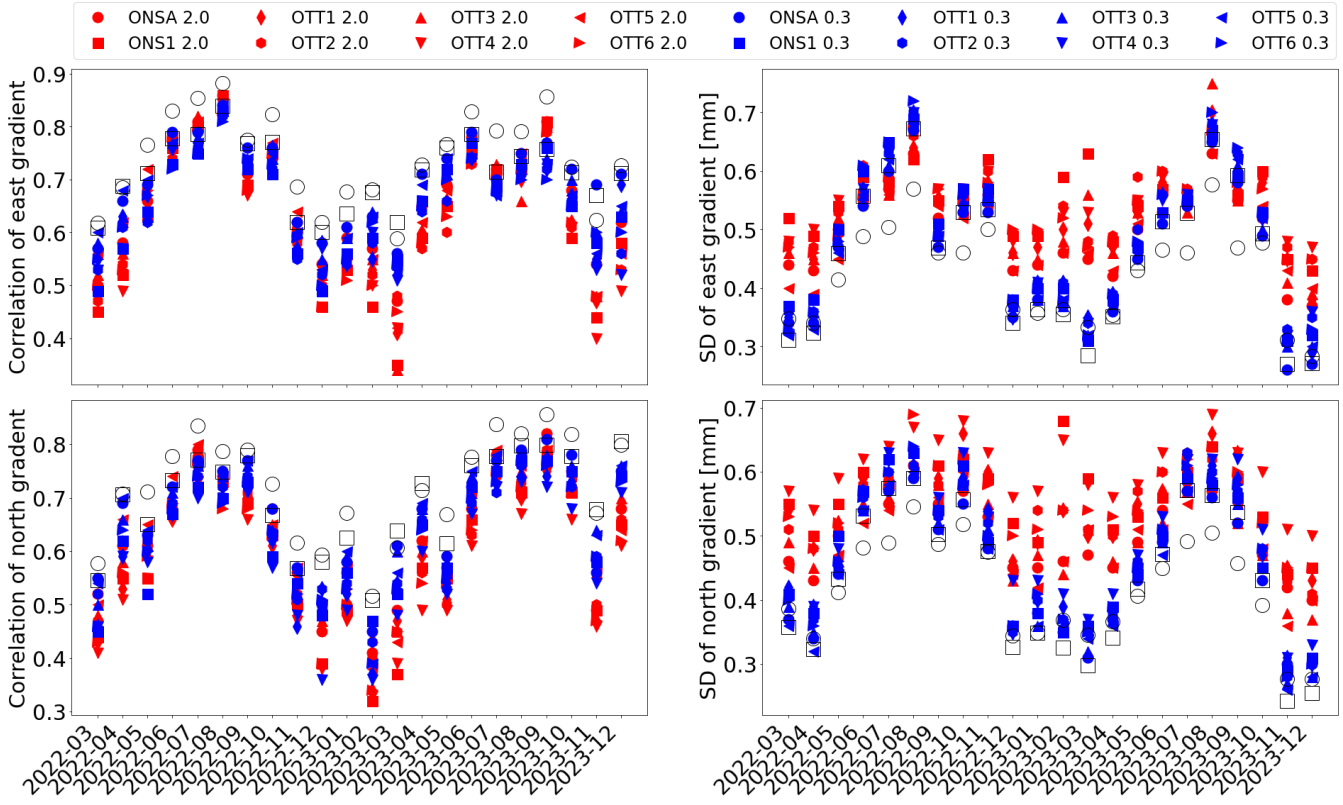


**Figure 8.** The correlation (left) and standard deviation (right) between the GNSS and the WVR gradients for each month when two different constraints are applied in the GNSS data processing. The values from the averaged GNSS data are shown by black circles for the constraint of 2.0 mm$\sqrt{\text{h}}^{-1}$ and by black squares for the constraint of 0.3 mm$\sqrt{\text{h}}^{-1}$.

## 4 Conclusions

The linear horizontal gradients covering a nearly two-year period were estimated from eight co-located GNSS stations using data acquired from GPS, GLONASS, Galileo, and BeiDou satellites. When the gradients obtained from the GNSS stations were compared to each other we see consistent agreements across all stations, including OTT5, where the antenna is mounted directly above the bedrock. This is probably due to that a plate of microwave absorbing material was placed right below the antenna. A slightly worse agreement is observed for station OTT4 compared to the others due to the station's proximity to one of the geodetic VLBI telescopes, resulting in the loss of observations at low elevation angles in the south-south-east direction.

The GNSS-derived gradients were also compared to the ones obtained from a co-located WVR. A better agreement is obtained when using WVR data with a liquid water content (LWC) less than 0.05 mm compared to when LWC values of up to 0.7 mm are included. However, a smaller LWC threshold results in a 35 % reduction in the available WVR data points.

https://doi.org/10.5194/egusphere-2024-2716
Preprint. Discussion started: 2 October 2024


Therefore, in some applications it may be important to balance the amount of available data for tracking the variability of gradients under as many different weather conditions as possible and the accuracy of the data.

We found that the different constraints applied in GipsyX data processing have clear impact on the resulting gradient estimation. A weak constraint of 2.0 mm$\sqrt{\text{h}}^{-1}$ helps the GNSS data to track short-lived gradients, however at the cost of increased formal errors. This may be desirable for applications with a higher tolerance for formal errors but a greater focus on tracking the variability of water vapour. For instance, according to the product requirements from the EIG EUMETNET GNSS Water Vapour Programme (E-GVAP), the threshold value for the formal error of the near real-time Zenith Total Delay (ZTD) product is 15 mm. This threshold ensures that the ZTD product can be assimilated into numerical weather forecasting models (Dymarska et al., 2017).

The result also shows that the averaged GNSS gradients from eight co-located stations can significantly reduce the random noise introduced by a weak constraint and outperforms the undifferentiated gradients from a single station in terms of correlation and standard deviation when compared to the WVR data. This fusion approach can be used in order to obtain a more reliable variability of the water vapour for a GNSS station which can be applied as more suitable constraint for future GNSS data processing. Such an approach can also be applied to a single GNSS station with multiple receivers connected to the same antenna (Kačmařík et al., 2019).

*Acknowledgement.* The geodetic research infrastructure at the Onsala Space Observatory is funded by Swedish Mapping, Cadastral and Land Registration Authority and Chalmers University of Technology.

*Data availability.* The estimated gradients from the GNSS and the WVR data will be registered and archived by the Swedish National Data Service (SND) if and when the paper is accepted for publication. Before that these data are made available by the authors.

*Author contributions.* The two authors (TN and GE) planned the work and the structure of the paper together. TN performed the GNSS data analyses and GE performed the WVR data analyses. Both contributed to the writing of the manuscript and approved it before the submission.

*Competing interests.* The authors declare that they have no conflict of interest.

https://doi.org/10.5194/egusphere-2024-2716
Preprint. Discussion started: 2 October 2024


**Table 5.** Agreement between the horizontal gradients from mutli-GNSS and WVR. The best and the worst agreements are highlighted by cyan and red colour, respectively.

| Station | Constraint of 0.3 mm$\sqrt{\text{h}}^{-1}$ | | | | Constraint of 2.0 mm$\sqrt{\text{h}}^{-1}$ | | | |
|---|---|---|---|---|---|---|---|---|
| | Correlation | | RMS | | Correlation | | RMS | |
| | EG | NG | EG [mm] | NG [mm] | EG | NG | EG [mm] | NG [mm] |
| *All gradients* | | | | | | | | |
| ONSA | 0.71 | 0.69 | 0.69 | 0.50 | 0.68 | 0.66 | 0.71 | 0.55 |
| ONS1 | 0.67 | 0.64 | 0.72 | 0.53 | 0.64 | 0.61 | 0.77 | 0.61 |
| OTT1 | 0.69 | 0.63 | 0.70 | 0.53 | 0.66 | 0.62 | 0.73 | 0.59 |
| OTT2 | 0.67 | 0.65 | 0.74 | 0.52 | 0.65 | 0.63 | 0.77 | 0.59 |
| OTT3 | 0.69 | 0.67 | 0.66 | 0.50 | 0.66 | 0.65 | 0.68 | 0.55 |
| OTT4 | 0.66 | 0.62 | 0.70 | 0.54 | 0.64 | 0.59 | 0.76 | 0.63 |
| OTT5 | 0.68 | 0.67 | 0.67 | 0.50 | 0.67 | 0.66 | 0.69 | 0.54 |
| OTT6 | 0.66 | 0.65 | 0.72 | 0.54 | 0.64 | 0.62 | 0.75 | 0.61 |
| Fusion | 0.71 | 0.70 | 0.68 | 0.50 | 0.74 | 0.74 | 0.66 | 0.47 |
| *WVR total gradients $>$ 0.5 mm* | | | | | | | | |
| ONSA | 0.75 | 0.75 | 0.84 | 0.59 | 0.75 | 0.74 | 0.83 | 0.61 |
| ONS1 | 0.72 | 0.70 | 0.88 | 0.63 | 0.72 | 0.69 | 0.89 | 0.67 |
| OTT1 | 0.73 | 0.70 | 0.84 | 0.62 | 0.72 | 0.69 | 0.85 | 0.65 |
| OTT2 | 0.72 | 0.71 | 0.88 | 0.62 | 0.72 | 0.71 | 0.89 | 0.64 |
| OTT3 | 0.73 | 0.73 | 0.80 | 0.60 | 0.73 | 0.73 | 0.79 | 0.61 |
| OTT4 | 0.71 | 0.68 | 0.87 | 0.64 | 0.71 | 0.67 | 0.87 | 0.68 |
| OTT5 | 0.72 | 0.73 | 0.83 | 0.60 | 0.73 | 0.73 | 0.81 | 0.60 |
| OTT6 | 0.71 | 0.71 | 0.87 | 0.64 | 0.71 | 0.70 | 0.87 | 0.68 |
| Fusion | 0.75 | 0.75 | 0.84 | 0.59 | 0.79 | 0.80 | 0.79 | 0.55 |
| *WVR total gradients $<$ 0.5 mm* | | | | | | | | |
| ONSA | 0.33 | 0.28 | 0.36 | 0.31 | 0.28 | 0.25 | 0.47 | 0.44 |
| ONS1 | 0.31 | 0.22 | 0.39 | 0.34 | 0.24 | 0.20 | 0.56 | 0.51 |
| OTT1 | 0.34 | 0.20 | 0.37 | 0.35 | 0.28 | 0.20 | 0.51 | 0.49 |
| OTT2 | 0.31 | 0.24 | 0.41 | 0.33 | 0.26 | 0.21 | 0.55 | 0.49 |
| OTT3 | 0.31 | 0.25 | 0.34 | 0.32 | 0.25 | 0.23 | 0.48 | 0.44 |
| OTT4 | 0.30 | 0.22 | 0.37 | 0.36 | 0.25 | 0.20 | 0.53 | 0.55 |
| OTT5 | 0.34 | 0.24 | 0.33 | 0.32 | 0.29 | 0.22 | 0.44 | 0.44 |
| OTT6 | 0.33 | 0.25 | 0.36 | 0.33 | 0.26 | 0.21 | 0.51 | 0.51 |
| Fusion | 0.37 | 0.28 | 0.33 | 0.29 | 0.35 | 0.30 | 0.39 | 0.34 |

https://doi.org/10.5194/egusphere-2024-2716
Preprint. Discussion started: 2 October 2024


## References

Bar-Sever YE, Kroger PM, and Börjesson JA (1998) Estimating horizontal gradients of tropospheric path delay with a single GPS receiver, J. Geophys. Res., 103(B3), 5019–5035, https://doi.org/10.1029/97jb03534.

Bertiger W, Bar-Sever Y, Dorsey A et al. (2020) GipsyX/RTGx, a new tool set for space geodetic operations and research, Adv. Space Res., 66:469–489, https://doi.org/10.1016/j.asr.2020.04.015.

Boehm J, Werl B, and Schuh H (2006) Troposphere mapping functions for GPS and very long baseline interferometry from European Centre for Medium-Range Weather Forecasts operational analysis data, J. Geophys. Res., 111:B02406, https://doi.org/10.1029/2005JB003629.

Chen B, and Liu Z (2016) Global water vapor variability and trend from the latest 36 year (1979 to 2014) data of ECMWF and NCEP reanalyses, radiosonde, GPS, and microwave satellite, J. Geophys. Res. Atmos., 121:11,442–11,462, https://doi.org/10.1002/ 2016JD024917, 2016.

Davis, J. L., Elgered, G., Niell, A. E., and Kuehn, C. E.: Ground-based measurement of gradients in the "wet" radio refractivity of air, Radio Sci., 28(6), 1,003–1,018, https://doi.org/10.1029/93RS01917, 1993.

Dymarska N, Rohm W, Serny J, Kaplon J, Kubik T, Kryza M, Jutarski J, Gierczak J, and Kosierb R (2017) An assessment of the quality of near-real time GNSS observations as a potential data source for meteorology, Meteorology Hydrology and Water Management, 5:3-13, https://doi.org/10.26491/mhwm/65146.

Elgered G, Ning T, Forkman P, and Haas R (2019) On the information content in linear horizontal delay gradients estimated from space geodesy observations, Atmos Meas Tech, 12:3805–3823, https://doi.org/10.5194/amt-12-3805-2019

Emardson TR, Johansson JM, and Elgered G (2000) The systematic behavior of water vapor estimates using four years of GPS observations. Trans. IEEE Geosci. Remote Sens., 38:324–329, https://doi.org/10.1109/36.823927.

Jarlemark POJ, Emardson TR, and Johansson JM (1998) Wet delay variability calculated from radiometric measurements and its role in space geodetic parameter estimation, Radio Sci., 33:719–730, https://doi.org/10.1029/98RS00551.

Kačmařík M, Douša J, Zus F, Václavovic P, Balidakis K, Dick G, and Wickert J (2019) Sensitivity of GNSS tropospheric gradients to processing options, Ann. Geophys., 37:429–446, https://doi.org/10.5194/angeo-37-429-2019.

Kierulf HP, Steffen H, Barletta VR, Lidberg M, Johansson J, Kristiansen O, Tarasov L (2021) A GNSS velocity field for geophysical applications in Fennoscandia, J. Geodyn., 146, 101845 (2021) https://doi.org/10.1016/j.jog.2021.101845

Lindskog M, Ridal M, Thorsteinsson S, and Ning T (2017) Data assimilation of GNSS zenith total delays from a Nordic processing centre, Atmos. Chem. Phys., 17:13,983–13,998, https://doi.org/10.5194/acp-17-13983-2017.

Ning T, Elgered G, and Johansson JM (2011) The impact of microwave absorber and radome geometries on GNSS measurements of station coordinates and atmospheric water vapour, Adv. Space. Res., 47(2):186–196, https://doi.org/10.1016/j.asr.2010.06.023.

Ning T, Wang J, Elgered G et al. (2016) The uncertainty of the atmospheric integrated water vapour estimated from GNSS observations, Atmos. Meas. Tech., 9:79–92, https://doi.org/10.5194/amt-9-79-2016.

Ning T, and Elgered G (2021) High-temporal-resolution wet delay gradients estimated from multi-GNSS and microwave radiometer observations, Atmos. Meas. Tech., 14:5593–5605, https://doi.org/10.5194/amt-14-5593-2021.

Parracho AC, Bock O, and Bastin S (2018) Global IWV trends and variability in atmospheric reanalyses and GPS observations, Atmos. Chem. Phys., 18:16,213–16,237, https://doi.org/10.5194/acp-18-16213-2018.

Prange L, Villiger A, Sidorov D et al. (2020) Overview of CODE's MGEX solution with the focus on Galileo, Adv. Space. Res., 66:2786–2798, https://doi.org/10.1016/j.asr.2020.04.038.

https://doi.org/10.5194/egusphere-2024-2716
Preprint. Discussion started: 2 October 2024


Thundathil R, Zus F, Dick G et al. (2024) Assimilation of GNSS tropospheric gradients into the Weather Research and Forecasting (WRF) model version 4.4.1, Geosci. Model Dev., 17:3599–3616, https://doi.org/10.5194/gmd-17-3599-2024.

re3data.org: VMF Data Server; editing status 2024-05-15; re3data.org - Registry of Research Data Repositories, https://doi.org/10.17616/R3RD2H.

Wang R, Marut G, Hadas T, Hobiger T (2024) Improving GNSS meteorology by fusing measurements of several colocated receivers on the observation level, IEEE J. Sel. Top. Appl. Earth Obs. Remote Sens. 17:7841–7851, https://doi.org/10.1109/JSTARS.2024.3381792.

Zumberge JF, Heflin MB, Jefferson DC et al. (1997) Precise Point Positioning for the Efficient and Robust Analysis of GPS Data from Large Networks, J. Geophys. Res., 102 (B3), 5005–5017, https://doi.org/10.1029/96JB03860.